2014

Interface strain-induced multiferroicity in a SmFeO3 film

Zhenxiang Cheng
University of Wollongong, cheng@uow.edu.au

Fang Hong
University of Wollongong, fh640@uowmail.edu.au

Yuanxu Wang
Henan University

Kiyoshi Ozawa
National Institute for Materials Science, Japan

Hiroki Fujii
National Institute for Materials Science, Japan

See next page for additional authors

Publication Details

Cheng, Z., Hong, F., Wang, Y., Ozawa, K., Fujii, H., Kimura, H., Du, Y., Wang, X. & Dou, S. (2014). Interface strain-induced multiferroicity in a SmFeO3 film. ACS Applied Materials and Interfaces, 6 (10), 7356-7362.

Interface strain-induced multiferroicity in a SmFeO3 film

Abstract
An epitaxial pseudocubic SmFeO3 thin film on (100) Nb-SrTiO 3 was studied based on ferroelectric (FE) characterization and magnetic measurements. High-resolution transmission electron microscopy images clarify the nature of the epitaxial growth, the stress-induced structural distortion at the film/substrate interface, and the existence of two different orientation lattices. Clear grain boundaries can be seen, which could introduce an extra local distortion. Rectangular FE loops can be observed at room temperature, even by just applying a small voltage ranging from -1 to +1 V, indicative of the presence of FE polarization. Piezoelectric force microscopy images confirm the existence of FE domains and the switchable polarization. A strong ferromagnetic-like transition occurs around 185 K, which is much lower than the transition observed in the bulk sample. It is believed that the pseudocubic structure enhances FE polarization and decreases the magnetic ordering temperature, which is confirmed by the first-principles theoretical calculations. Meanwhile, the ferroelectricity in this thin film should originate from distortion and modification in the structural modules rather than from the exchange striction interaction that is found in the bulk SmFeO3.

Keywords
multiferroicity, smfeo3, induced, film, strain, interface

Disciplines
Engineering | Physical Sciences and Mathematics

Publication Details
Cheng, Z., Hong, F., Wang, Y., Ozawa, K., Fujii, H., Kimura, H., Du, Y., Wang, X. & Dou, S. (2014). Interface strain-induced multiferroicity in a SmFeO3 film. ACS Applied Materials and Interfaces, 6 (10), 7356-7362.

Authors
Zhenxiang Cheng, Fang Hong, Yuanxu Wang, Kiyoshi Ozawa, Hiroki Fujii, Hideo Kimura, Yi Du, Xiaolin Wang, and S X. Dou

Interface Strain induced multiferroicity in $SmFeO_3$ film

Zhenxiang Cheng[1], Fang Hong[1], Yuanxu Wang[2], Kiyoshi Ozawa[3], Hiroki Fujii[3], Hidoe Kimura[3], Yi Du[1], Xiaolin Wang[1], Shixue Dou[1]*

[1]Institute for Superconducting and Electronics Materials, University of Wollongong, Innovation Campus, North Wollongong, NSW 2519, Australia

[2]Institute for Computational Materials Science, School of Physics and Electronics, Henan University, Kaifeng, 475004, People's Republic of China

[3]National Institute for Materials Science, Sengen 1-2-1, Tsukuba, Japan

Epitaxial pseudocubic $SmFeO_3$ thin film on (100) Nb-$SrTiO_3$ was studied based on ferroelectric (FE) characterization and magnetic measurements. High resolution transmission electron microscope images clarify the nature of the epitaxial growth, the stress induced structural distortion at the film/substrate interface, and the existence of two different orientation lattices. Clear grain boundaries can be seen, which could introduce an extra local distortion. Rectangular FE loops can be observed at room temperature, even by just applying a small voltage ranging from -1 V to 1 V, indicative of the presence of ferroelectric polarization. Piezoelectric force microscope images confirm the existence of ferroelectric domains and the switchable polarization. A strong ferromagnetic-like transition occurs around 185 K, which is much lower than the transition observed in the bulk sample. It is believed that the pseudocubic structure enhances ferroelectric polarization and decreases the magnetic ordering temperature, which is confirmed by the first principles theoretical calculations. Meanwhile, the ferroelectricity in this thin film should originate from distortion and modification in the structural modules rather than from the exchange striction interaction that is found in the bulk $SmFeO_3$.

Corresponding author, email: cheng@uow.edu.au,

INTRODUCTION

The wide application of traditional data storage is attributed to the giant magnetoresistance effect [1, 2]. Due to increasing demands for more computing power and data storage, a new type of unit cell with higher data density and lower power consumption is required. Ferroelectric random access memory seems to be a good choice, in which vertical polarization can be easily achieved, meaning that high density could be obtained. Meanwhile, the stability of ferroelectric domains ensures that information can be well saved for a long time. On the other hand, one special type of material in which magnetic ordering and ferroelectric ordering can coexist, the so-called multiferroic materials, also shows great potential for the next generation of data storage applications and other kinds of spintronic devices because spin freedom can be operated beyond the charge freedom. Therefore, exploring new functional materials having multiferroic properties has been a highly topical research field in recent years[3-7]. $BiFeO_3$ has shown its priority due to its room temperature multiferroic property.[8] Bi^{3+} is not friendly to the environment or to human health, however, and to obtain single phase on a large scale is still a problem, which could increase the cost of production. Furthermore, the weak magnetization at room temperature, weak magnetoelectric coupling, and large electrical coercive field strongly limits its practical application. Rare earth manganites, such as $DyMnO_3$[9-11] and $TbMnO_3$[10] (space group: *Pnma*), are of great interest, as electric polarization is induced by spiral magnetic ordering because of the simultaneously broken spatial inversion and time-reversal symmetries.[12] In addition, the FE property can also be found in antiferromagnetic hexagonal $HoMnO_3$ and $YMnO_3$ (space group: $P6_3cm$).[13, 14] The FE property of these two materials originates from the buckling of layered MnO_5 polyhedral units, driven by the size effect and electrostatic interaction as well. In these manganites, the spiral magnetic ordering temperatures are very low and far away from room temperature, which restricts their application at common ambient temperatures. Most traditional ferroelectric materials, such as lead zirconate titanate (PZT) and $BaTiO_3$, are not magnetic. Therefore, to find new multiferroic materials with strong ferroelectricity and a high magnetic transition temperature seems to be the unavoidable way to achieve real applications. Up to now, there have been few reports on ferroelectric studies of the orthoferrites, except for $DyFeO_3$ and $SmFeO_3$.[15-17]From the point of view of symmetry, it is nearly impossible to achieve a ferroelectric phase in orthorhombic ferrite. In the case of $DyFeO_3$, the ferroelectric transition takes place below the magnetic transition temperature of the Dy^{3+} lattice around 3.5 K, which can be explained by the exchange-striction interaction. As for $SmFeO_3$, a small polarization is supposed to occur due to the symmetric exchange striction interaction among the canted antiferromagnetic spins[18, 19], so it shares similar ferroelectric origins to $DyFeO_3$[15] and $CaMn_7O_{12}$[20-22]. Strain engineering has been employed to produce low dimensional materials such as functional thin films, and this method has introduced many unique properties which are not possessed by their corresponding bulk forms. Recently, ferroelectricity has been reported in artificially hexagonal $YbFeO_3$ thin film on a hexagonal substrate.[23] In this work, however, we study epitaxial pseudocubic $SmFeO_3$ on (001) $SrTiO_3$ (STO):Nb substrate prepared by pulsed laser deposition. Assuming that the mismatch between the two sets of lattices could introduce strain and lead to local structural distortion at the film/substrate interface, the structure and the physical properties of the thin film may consequently be modified. Our characterization shows that a ferroelectric loop is present at room temperature, and piezoresponse force microscope images confirm the switchable ferroelectric domain structure. Meanwhile, magnetic measurement results show that the $SmFeO_3$ experiences a ferromagnetic-like (canted antiferromagnetic) transition around 185 K, quite different from bulk $SmFeO_3$, which is indicative of the multiferroic property in this material. Transmission electron microscopy (TEM) confirms the local structural distortion induced by the strain effect and consequent symmetry change at the film/substrate interface. First principles calculations confirm ferroelectric polarization in the pseudocubic distorted $SmFeO_3$ film.

EXPERIMENTAL

$SmFeO_3$ thin films were deposited at 830℃ on (001) Nb-STO in a dynamic flowing oxygen atmosphere of 200 mTorr, using a pulsed laser deposition (PLD) system. The $SmFeO_3$ target was prepared by the solid state reaction method, and X-ray diffraction (XRD, model: GBC MMA, Cu Kα radiation) shows that it is single phase with orthorhombic structure. A Nd:YAG laser source was used with 355 nm wavelength. During the deposition process, the laser was stabilized at 6-7 J/cm^2, and pulses were repeated at 10 cycles per second. The crystal structures of the films were examined by XRD at room temperature. The thickness of the films was determined by scanning electron microscope (SEM, model: JEOL JSM-6460A) and is around 450 nm. A high resolution transmission electron microscope (HRTEM, model: JEOL JEM-4000EX) clarified the epitaxial growth of the thin film at the interface and the existence of boundaries which separate the majority $[010]_o$ and the minority $[101]_o$ lattices. Magnetic properties were measured by a superconducting quantum interference device (SQUID) magnetometer. Pt electrodes were deposited on the film for ferroelectric measurements by magnetron sputtering with a standard shadow mask. A Ferroelectric Analyser (TF2000, aixACCT) was employed to characterize the ferroelectric properties (ferroelectric hysteresis loops and fatigue). Meanwhile, PUND mode measurements were performed to reveal the real switching process. Nanoscale ferroelectric measurements of as-grown $SmFeO_3$ film were carried out via piezoresponse force microscopy (PFM, model: MFP-3D Asylum Research). The typical scan size and rate were 500 nm and 0.1 Hz,

respectively. Positive and negative dc bias of 5 V was applied to the tip to produce the switched domain structure, and subsequent scanning was done at 370 kHz in dual AC resonance tracking (DART) PFM mode.

For the first principles calculations, an initial distorted structure was used. The redefined crystal axes of the $SmFeO_3$ film were set as: $a//[10\bar{1}]_o$, $b//[010]_o$, and $c//[101]_o$ of the orthorhombic structure of bulk $SmFeO_3$. The lattice parameters a and b of the film were set as $a = b = 7.81$ Å $= 2c$ for the STO, while the out-of-plane lattice parameter c and angle β were relaxed. During this process, other parameters, a, b, and the angles α and γ were fixed. The relaxed and distorted $SmFeO_3$ crystal structure is $a = b = 7.81$ Å, $c = 7.44$ Å, $\alpha = 90^o$, $\beta = 92.09^o$ and $\gamma = 90^o$. The calculations were performed using the project-augmented wave (PAW) method implemented in the Vienna ab initio simulation package (VASP).

RESULTS AND DISCUSSION

The $SmFeO_3$ (SFO) thin film was prepared by pulsed laser deposition on (001) STO:Nb single crystal substrate. The basic structure was examined by X-ray diffraction (XRD), as shown in Figure 1. The XRD pattern reveals that the $SmFeO_3$ is epitaxially grown, and three satellite peaks are found near the (001), (002), and (003) STO:Nb peaks. This is similar to the case of $LuFeO_3$ and $BiFeO_3$ films on (001) STO substrate, which are both "cube-on-cube", grown epitaxially with pseudocubic structure. According to these three diffraction peaks, we can estimate the out-of-plane pseudocubic lattice parameter as $a = 3.72$ Å. Considering the similarity between epitaxial $BiFeO_3$[24, 25] and $SmFeO_3$, it is reasonable to tentatively assign the $SmFeO_3$ film to the rhombohedral or hexagonal structure. A structural study based on diffraction peak calculations shows that the three peaks of the pseudocubic structure can successfully be assigned to the (012), (024), and (217) peaks of the rhombohedral structure (*R3c*, $a_r = 5.638$ Å, $\alpha_r = 52.64$ °), or to the (102), (204), and (217) peaks of the hexagonal structure (*P6₃cm*, $a_h = b_h = 5.00$ Å, $c_h = 14.53$ Å, $\alpha = \beta = 90°$, $\gamma = 120°$).

Compared with the sharp diffraction peaks from the substrate, the three peaks from the thin film are relatively broad, which may originate from two sets of reflections from close sets of lattice parameters. To find out how the thin film really grows, high resolution transmission electron microscopy (HRTEM) was employed to determine the interface structure, as shown in Figure 2. The cross-section of the thin film was imaged in bright-field mode, in which a clear interface between the thin film and the substrate can be seen. In Figure 2, a specifically selected film/substrate interface highlighted in the dotted rectangular frame is magnified in the upper left corner.

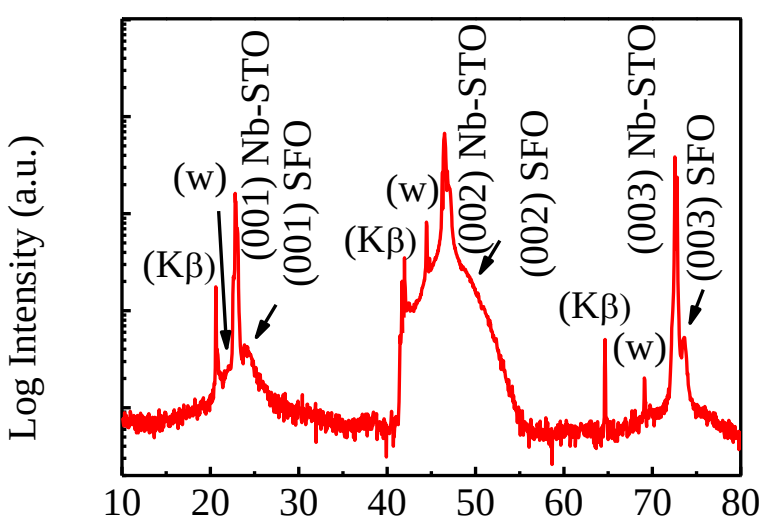

Fig. 1 X-ray diffraction pattern of $SmFeO_3$ film deposited on (001) STO:Nb single crystal substrate; lattice parameter: STO c_c=3.905 and SFO c_c=3.790.

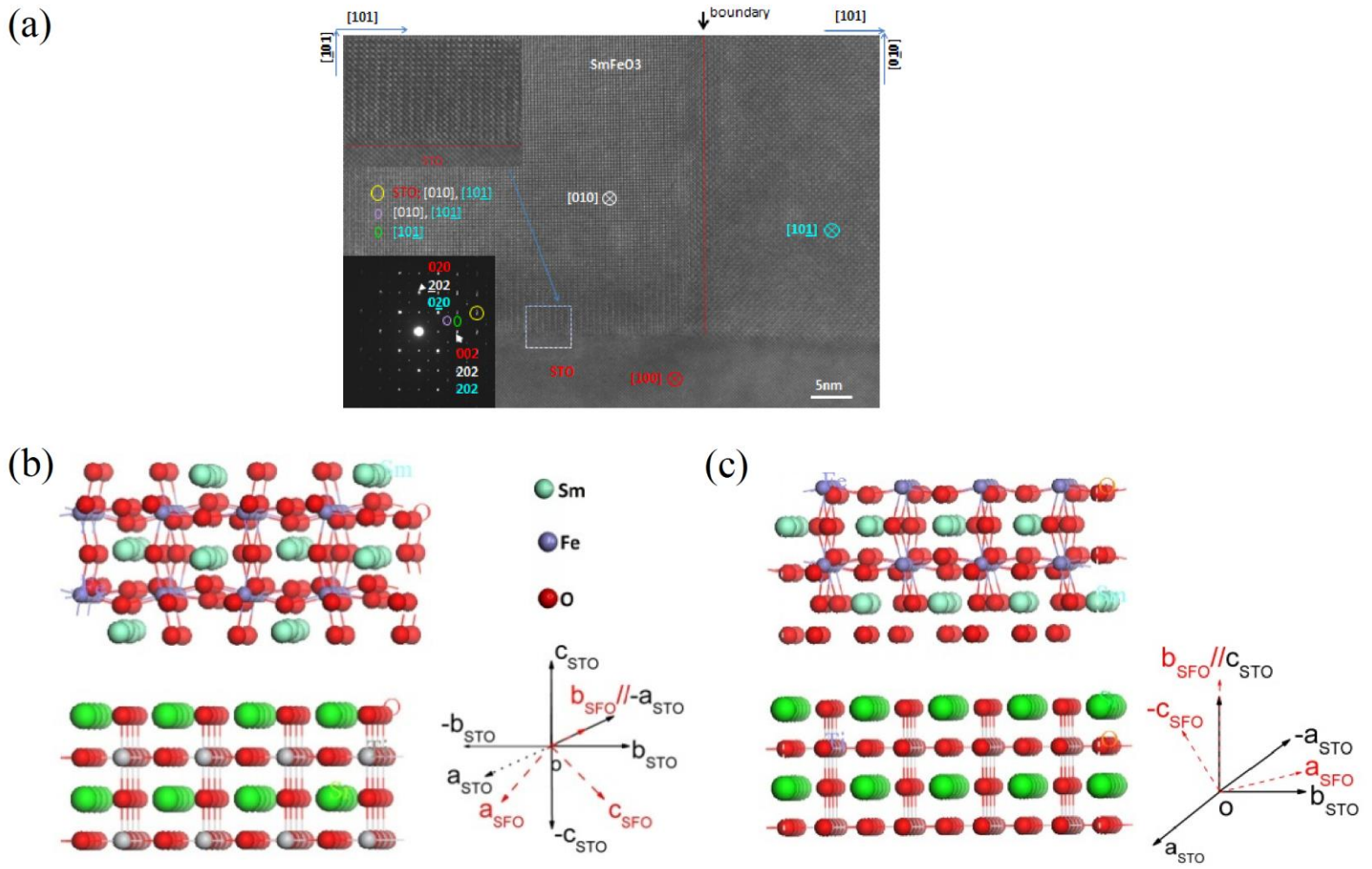

Fig. 2 (a) Interface between the $SmFeO_3$ thin film and the STO substrate, on which the grain boundary of $[010]_o$ and $[101]_o$ grains is also shown. The inset in the upper left corner is the HRTEM image of the film/substrate interface, magnified from the selected [010] growth area shown in the dotted rectangular frame. The inset in the lower left corner is the selected area electron diffraction pattern, where the high level diffraction spot shows a splitting, indicating the different structures existing in the film. (b) and (c) contains the schematic structures of the two different growth orientations of the film, $<101>_o$ and $<010>_o$, respectively.

Considering the lattice mismatch between the orthorhombic $SmFeO_3$ and the cubic STO, stress induced distortion should exist at the film/substrate interface. The TEM image of the film/substrate interface clearly shows the atomic rearrangement in an exactly cubic structure that is gradually relaxed to orthorombic. In addition, two types of growth along different crystallographic directions of orthorhombic $SmFeO_3$ were found. A structural transition boundary is clearly shown in the TEM image. According to the TEM image and the selected area electron diffraction pattern, the growth direction of the $SmFeO_3$ film in relation to the substrate orientation can be determined, which is shown in Fig. 2(b) and (c). The out-of-plane directions of the $SmFeO_3$ film on (100) STO substrate are $<101>_o$ and $<010>_o$, respectively. Therefore the three satellite diffraction peaks in the XRD patterns from low to high angles can be assigned to $1/2(101)_o$, $(101)_o+(010)_o$, and $3/2(101)_o$. This also explains why the diffraction peak of the film at around $2\theta = 48^o$ is broad, because it contains two sets of diffraction peaks in very close positions. The estimated lattice spacing d_{101} is 3.79 Å, which is significantly reduced in comparison with the bulk value of 3.89 Å. Such a reduction is caused by elongation of the *b* axis due to the fact that b_{SFO} = 7.706Å which is less than $2a$ = 7.806 Å of STO. This estimation is based on the part of the film with $<101>_o$ growth, although the part of the film with $<010>_o$ growth may not exhibit a significant change in the lattice parameter because the in-plane d_{101} lattice spacing matches well with d_{100} of the STO substrate. Therefore, the so-called epitaxial growth actually includes two sets of growth directions. The part of the film with $<101>_o$ growth shows significant distortion with reduced *a* and *c*, and elongated *b*. Such a structural distortion will cause orbital and spin reconstruction and result in novel properties.

The existence of the two sets of growth will introduce grain boundaries with disorder or rearrangement of the atoms, which can be clearly observed in the TEM image in Fig. 2. The boundary between the [010] and [101] lattices should also introduce extra stress and local structural distortion in this system. The epitaxial growth of the film will gradually relax, and therefore, the structural distortion will be released when the film grows thicker. The boundaries between lattices with two different orientations always exist, however, which is beyond the scale of the stress on the interface.

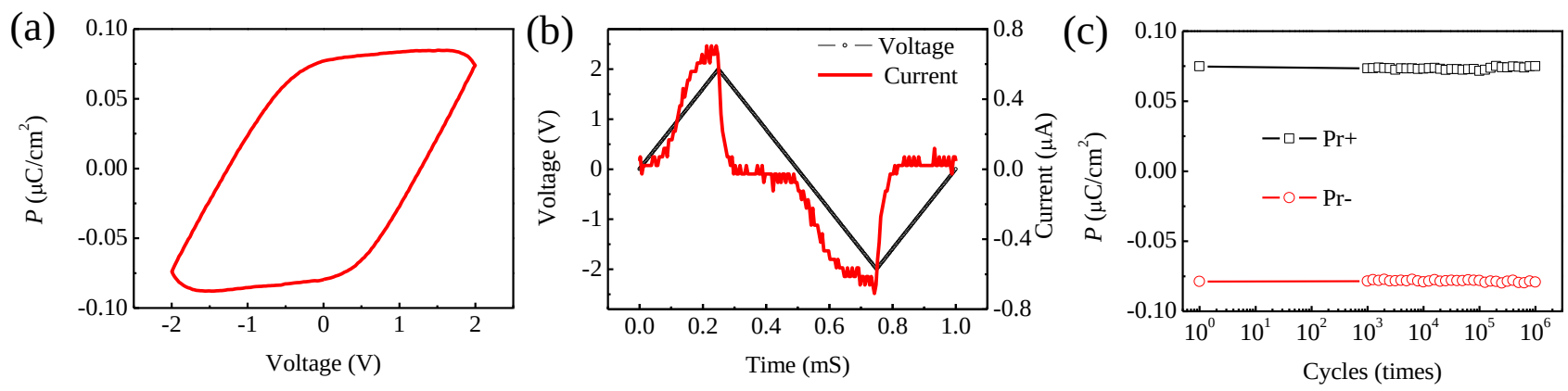

Fig. 3 (a) Electrical hysteresis loop of $SmFeO_3$ film on STO:Nb at room temperature, (b) time dependence of applied voltage and corresponding current, (c) fatigue test results after 10^6 cycles (10 data points every decade).

Electric hysteresis loops of $SmFeO_3$ films on STO:Nb were collected at room temperature. When the applied voltage exceeds 1.2 V (electric field ~22 kV/cm), a quasi-rectangular loop can be observed, as shown in Figure 3(a), indicating a strong FE property. A higher applied voltage will increase the leakage current, and a relatively round FE loop will be present (not shown). The time dependence of the applied voltage and consequent current are given in Figure 3(b), in which an obvious switching current can be seen, which is quite different from typical resistor or capacitor behaviour. The small difference in current behaviour between opposite voltages is probably due to the electrode effect (Au and Nb-STO). To check the fatigue properties, P-E loops were measured 10^6 times, and the remanent polarizations are presented in Figure 3(c). The remanent polarization is about 0.08 μC/cm^2. There was no significant change in the remanent polarization after the fatigue test, indicating the good stability of this FE material.

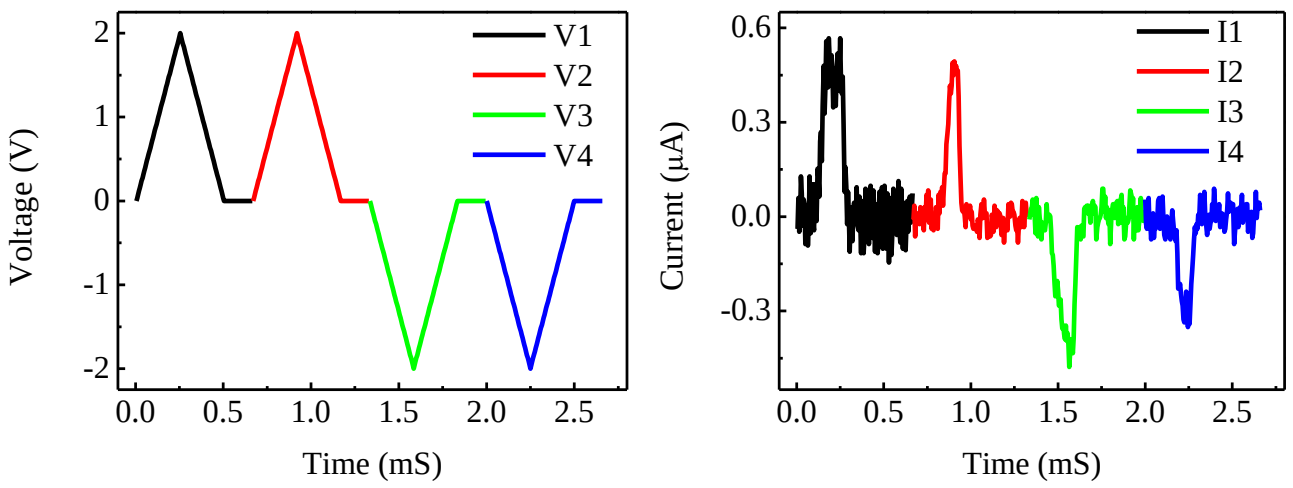

Fig. 4 Time dependence (left) of applied voltage (ranging from -2 V to 2 V) and consequent current (right) measured in the PUND mode.

Considering the leakage effect, which can also contribute to P-E loops, we used the positive-up negative-down (PUND) method to confirm the real polarization. The PUND method uses an up-up-down-down wave to exclude the leakage effect. The standard PUND wave form is presented in Figure 4. At the beginning, the system uses a negative writing pulse to polarize the film. After that, a positive pulse V1 is applied to the film, and a current will be produced due to leakage and domain flipping. Then, another positive pulse V2 is applied, and a current will be produced, but only due to leakage. Therefore, the integrity of the current difference produced between up-up or down-down processes is in accordance with two times the remanent polarization, $2P_r$. This also applies to the down-down process. A V3 pulse will switch the FE domains to the opposite direction, and V4 just measures the leakage current contribution. In Figure 3, a clear difference in the current between I1 and I2, or I3 and I4 can be observed (since the pure leakage current peak is lower and narrower than when it is combined with the switching current), indicating that polarization in the P-E loop is real. The real current contribution from FE switching is reduced to half, however, meaning that the remanent polarization is about 0.04 μC/cm^2. This value is very close to that found in orthorhombic $HoMnO_3$,[26, 27] in which Mn^{3+} spins are in E-type antiferromagnetic ordering. To some extent, considering the different magnetic states involved in the orthorhombic $HoMnO_3$ and the orthorhombic $SmFeO_3$, this similarity suggests that the mechanism in the orthorhombic bulk $SmFeO_3$ may not apply to the $SmFeO_3$ thin film.

The piezoelectric force microscope (PFM) image presented in Figure 5 shows the presence of FE domains, which are mainly dominated by two types with opposite vectors. This means that the domain walls in this film are mostly 180 °domain walls. Meanwhile, information on the surface morphology was also obtained, and the results show an average roughness of about 1.8 nm, indicative of good quality film. Comparing the morphology with the phase pattern, it is not difficult to see that there is more than one domain in some single grains. The average domain size is around 0.1 μm, much smaller than the domain size in $BiFeO_3$ film[28]. One important characteristic of the ferroelectricicity is that the ferroelectric domains can be controlled and reversed by external electric field, the so-called “write”. To do it, we carried out PFM lithography on the $SmFeO_3$ film. A square-in-square pattern is obtained, as shown in Figure 5(c), in which the inset is the pre-set pattern. The amplitude distribution along the red line across the pattern is presented in

Figure 5(d). It is clear that these two cubic boxes show opposite amplitude values, suggesting that they are truly two types of domains with opposite polarization directions.

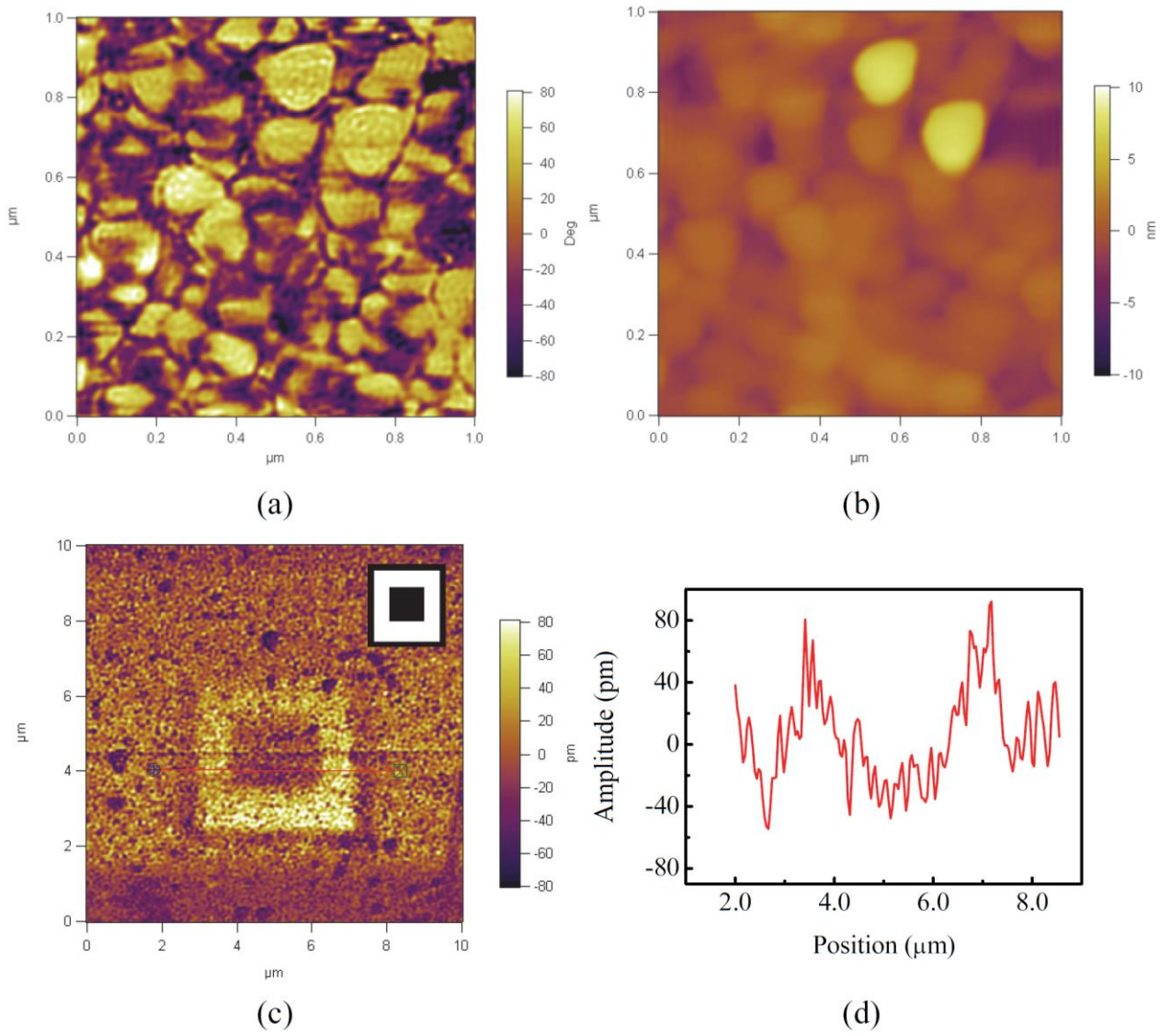

Fig. 5 Nanoscale ferroelectric domain structure characterized by PFM: (a) phase image and (b) morphology; (c) PFM lithography pattern, inset: the pre-set pattern, and (d) amplitude distribution along the red line across the lithography pattern in (c).

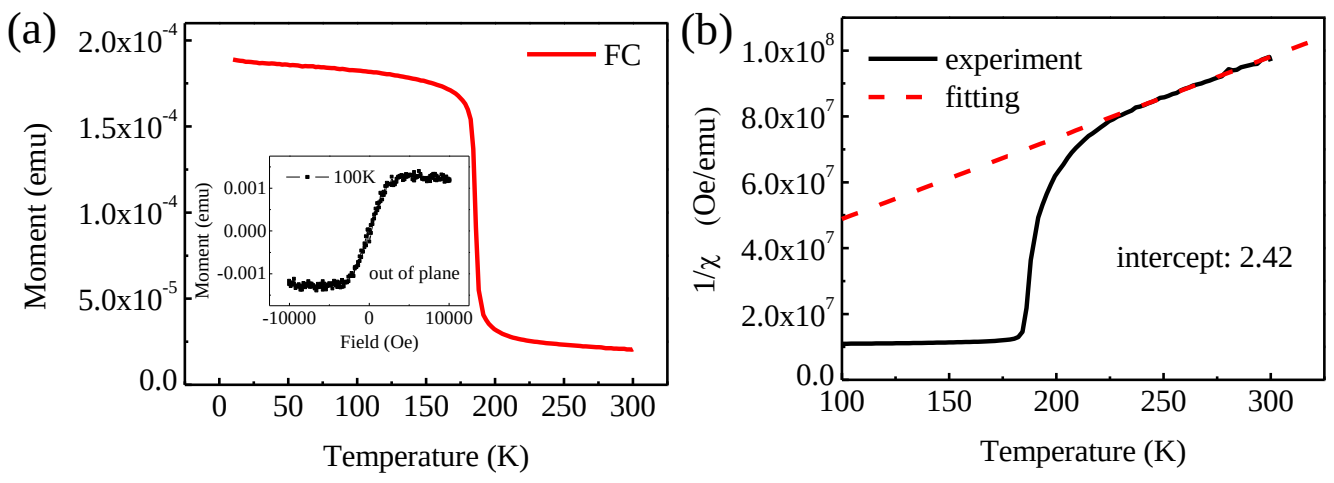

Fig. 6 (a) Temperature dependence of magnetic moment from 10 K to 300 K, and magnetic hysteresis loop measured at 100 K (inset); (b) antiferromagnetic interaction of Fe^{3+} sublattice confirmed by Curie-Weiss law fitting with temperature range from 100-300 K.

To investigate the magnetic properties of this "pseudocubic" $SmFeO_3$ film, we carried out measurements using a magnetic properties measurement system (MPMS). The field-cooling temperature dependence of the magnetic moment was measured from 10 K to 300 K, as shown in Figure 6 (a). A sharp ferromagnetic (FM)-like transition can be found around 185 K. The FM behaviour can be confirmed by the magnetic hysteresis loop at 100 K. Curie-Weiss law fitting gives a positive intercept, which corresponds to a negative Curie-Weiss temperature, indicating an antiferromagnetic (AFM) interaction starting below 240 K, as can been seen in Figure 6 (b). Hence, the FM-like behaviour should originate from a canted AFM ordering. This is quite different from what happens in bulk $SmFeO_3$, in which a spin reorientation takes place around 433 K from a canted antiferromagnetic weak ferromagnetic (WFM) ordering to simple antiferromagnetic ordering. Such a big change may be attributed to Fe^{3+} spin frustration, which weakens the interaction between Fe^{3+} ions compared with that in the orthorhombic lattice. The stress induced distortion on the interface and boundaries should be responsible for the significant change in the magnetic properties. This result indicates that the ferroelectricity in the $SmFeO_3$ at room temperature may be not arise from the magnetic exchange striction interaction, but from the structural distortion.

Table 1 Calculated total energies of the distorted $SmFeO_3$ system with different magnetic structures. The Hubbard-U values of 0 and 2 were considered in the calculation and compared. The ferroelectric polarization was calculated for G-type AFM.

	G-AFM	A-AFM	C-AFM	FM	PM	ΔP [100]
Energy*(U=0)	0	1.09	0.739	3.599	5.045	15.32 μC/cm^2
Energy*(U=2)	0	1.66	0.723	5.372	12.274	15.31 μC/cm^2

*Total energy (relative to the G-AFM state in eV/f.u.)

Bulk $SmFeO_3$ has been reported to show spin-driven ferroelectric polarization at room temperature based on experimental measurements, however, the theoretical calculations deny such a possibility. Therefore the multiferroic property in $SmFeO_3$ is still controversial. Our $SmFeO_3$ thin film, however, shows strong structural distortion at both the film/substrate interface and the grain boundaries. Such structural distortion will cause the reconstruction of the crystal lattice and rearrangement of spin, and thus electrical polarization, driven by both displacement of ions and spin. Adopting a distorted structure of $SmFeO_3$ at the film/substrate interface, the different magnetic states were calculated based on first principles calculations in the framework of density functional theory (DFT) and the result is presented in Table 1. The energies of those magnetic states were compared with G-type antiferromagnetic ordering of Fe for both Hubbard U = 0 and 2, which shows that G-AFM is the most stable state in comparison to A-type AFM, C-type AFM, FM, and paramagnetic (PM) states. The polarization is calculated as ~15.3 μC/cm^2 for both U values. The value of U does not show any significant effect on the magnetic state and polarization. Although the calculated polarization value is much larger than the measured value, this result indicates that the observed polarization might be caused by the structural distortion at the film/substrate interface. The discrepancy might be caused by the relaxation of the distorted $SmFeO_3$ film structure to a bulk one in a relatively thick film, which has been confirmed in high resolution TEM images. In addition, G-AFM easily forms a canted magnetic structure[29, 30] and causes the appearance of net moment and spin-driven polarization based on an inverse Dyaloshinski–Moriya (DM) interaction. Although we cannot distinguish the two contributions to the polarization, i.e., ionic-displacement-driven polarization and spin-driven polarization, studying the possibility for the existence of large magnetoelectric coupling will be the aim of the next step in our research program.

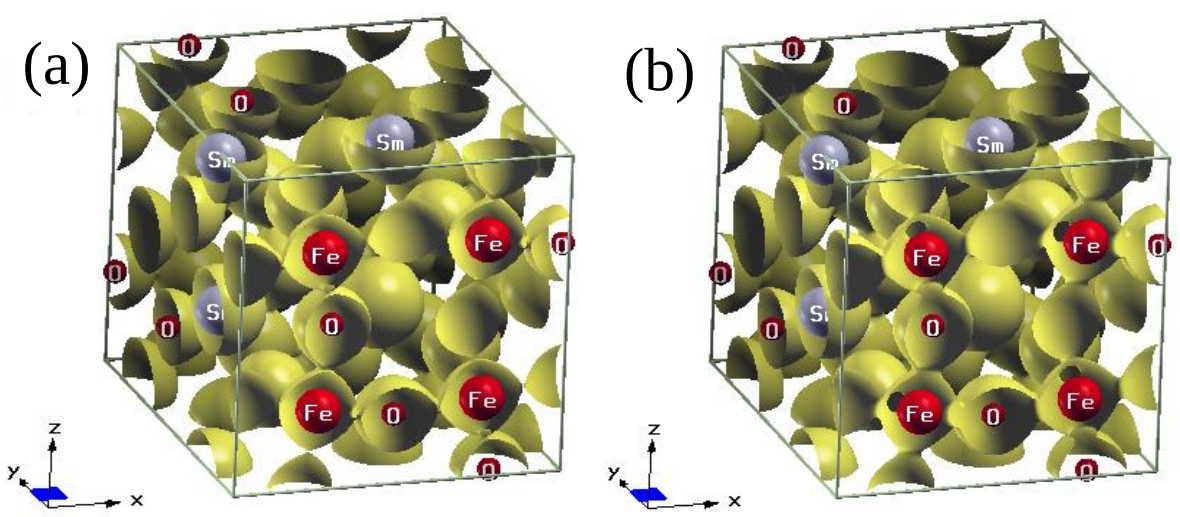

Fig.7 The calculated electron density isosurface with the value of 0.45 for undistorted (a) and distorted (b) $SmFeO_3$ systems.

Finally we compare the calculated electron density isosurface with the value of 0.45 for undistorted and distorted $SmFeO_3$ systems obtained from DFT calculation, which is shown in Figure 7. Electron density contour is known to be an informative tool to distingush different bonding interaction in solids. It is obversious that, in the distorted system, the electron density between oxygen and iron is strong to form a three dimensional network, indicating a strong asymmetric covalent bonding interaction. While in the undistorted sytstem, the electron density between oxygen and iron is weak. The strong asymmetric covalent bonding is responsable for the observaed polarization in the distorted $SmFeO_3$ thin film.

CONCLUSIONS

In summary, the structure, and the ferroelectric and magnetic properties were studied in epitaxial pseudocubic $SmFeO_3$ on STO: Nb substrate. Clear structural distortion can be identified on the $[010]_o$ grown film/substrate interface, as well as boundaries of $[010]_o$ and a small fraction of $[101]_o$ grains. A strong ferromagnetic-like transition is observed around 185 K, which is likely to be due to a canted antiferromagnetic ordering. The PFM images clarify the existence of ferroelectricity and the switchable domain structure. There is also a saturating hysteresis loop in the ferroelectric measurements, and the loops are very stable, even after 10^6 cycles. The PUND method was used to determine the intrinsic ferroelectric polarization, and the remanent polarization is about 0.04 μC/cm^2, which is comparable to that in orthorhombic $HoMnO_3$. The structural distortion in this system is probably responsible for the significant change in the magnetic properties and the small polarization as well. The theoretical calculations of the highly distorted $SmFeO_3$ structure have theoretically confirmed the existence of the ferroelectic polarization and net magnetic moment in the thin film form of $SmFeO_3$.

Acknowledgements

Zhenxiang Cheng thanks the Australian Research Council for support through a Future Fellowship (FT 0990287). We thank Dr. Tania Silver for carefully polishing the draft.

References

(1) Y. Moritomo, A. Asamitsu, H. Kuwahara, and Y. Tokura, *Nature* **1996**, 380, 141-144.

(2) M. B. Salamon and M. Jaime, *Reviews of Modern Physics* **2001**, 73, 583-628.

(3) G. Catalan and J. F. Scott, *Adv. Mater.* **2009**, 21, 2463-2485.

(4) C. A. F. Vaz, J. Hoffman, C. H. Anh, and R. Ramesh, *Adv. Mater.* **2010**, 22, 2900-2918.

(5) P. Jain, V. Ramachandran, R. J. Clark, H. D. Zhou, B. H. Toby, N. S. Dalal, H. W. Kroto, and A. K. Cheetham, *J. Am. Chem. Soc.* **2009**, 131, 13625-13627.

(6) H. Cui, Z. Wang, K. Takahashi, Y. Okano, H. Kobayashi, and A. Kobayashi, *J. Am. Chem. Soc.* **2006**, 128, 15074-15075.

(7) S. W. Kim, H. Y. Chang, and P. S. Halasyamani, *J. Am. Chem. Soc.* **2010**, 132, 17684-17685.

(8) Z.X. Cheng, X.L. Wang, S.X. Dou, K. Ozawa, H. Kimura, Phys. Rev. B **2008**, 77, 092101.

(9) N. Zhang, K. F. Wang, S. J. Luo, T. Wei, X. W. Dong, S. Z. Li, J. G. Wan, and J. M. Liu, *Appl. Phys. Lett.* **2010**, 96, 252902.

(10) T. Kimura, G. Lawes, T. Goto, Y. Tokura, and A. P. Ramirez, *Phys. Rev. B* **2005**, 71, 224425.

(11) T. Kimura, S. Ishihara, H. Shintani, T. Arima, K. T. Takahashi, K. Ishizaka, and Y. Tokura, *Phys. Rev. B* **2003**, 68, 060403.

(12) M. Mostovoy, *Phys. Rev. Lett.* **2006**, 96, 067601.

(13) H. Lueken, *Angewandte Chemie International Edition* **2008**, 47, 8562-8564.

(14) T. Matsumoto, R. Ishikawa, T. Tohei, H. Kimura, Q. Yao, H. Zhao, X. Wang, D. Chen, Z. Cheng, N. Shibata, and Y. Ikuhara, *Nano Letters* **2013**, 13, 4594-4601.

(15) Y. Tokunaga, S. Iguchi, T. Arima, and Y. Tokura, *Phys. Rev. Lett.* **2008**, 101, 097205.

(16) Y. Du, Z. X. Cheng, X. L. Wang, and S. X. Dou, *J. Appl. Phys.* **2010**, 107, 09D908.

(17) J.-H. Lee, Y. K. Jeong, J. H. Park, M.-A. Oak, H. M. Jang, J. Y. Son, and J. F. Scott, *Phys. Rev. Lett.* **2011**, 107, 117201.

(18) R. D. Johnson, N. Terada, and P. G. Radaelli, *Phys. Rev. Lett.* **2012**, 108, 219701.

(19) J.-H. Lee, Y. K. Jeong, J. H. Park, M.-A. Oak, H. M. Jang, J. Y. Son, and J. F. Scott, *Phys. Rev. Lett.* **2012**, 108, 219702.

(20) G. Zhang, S. Dong, Z. Yan, Y. Guo, Q. Zhang, S. Yunoki, E. Dagotto, and J. M. Liu, *Phys. Rev. B* **2011**, 84, 174413.

(21) R. D. Johnson, L. C. Chapon, D. D. Khalyavin, P. Manuel, P. G. Radaelli, and C. Martin, *Phys. Rev. Lett.* **2012**, 108, 067201.

(22) X. Z. Lu, M. H. Whangbo, S. Dong, X. G. Gong, and H. J. Xiang, *Phys. Rev. Lett.* **2012**, 108, 187204.

(23) Y. K. Jeong, J.-H. Lee, S.-J. Ahn, S.-W. Song, H. M. Jang, H. Choi, and J. F. Scott, *J. Am. Chem. Soc.* **2012**, 134, 1450-1453.

(24) M. K. Singh, H. M. Jang, S. Ryu, and M.-H. Jo, *Appl. Phys. Lett.* **2006**, 88, 042907-042903.

(25) J. F. Ihlefeld, A. Kumar, V. Gopalan, D. G. Schlom, Y. B. Chen, X. Q. Pan, T. Heeg, J. Schubert, X. Ke, P. Schiffer, J. Orenstein, L. W. Martin, Y. H. Chu, and R. Ramesh, *Appl. Phys. Lett.* **2007**, 91, 071922-071923.

(26) S. M. Feng, Y. S. Chai, J. L. Zhu, N. Manivannan, Y. S. Oh, L. J. Wang, Y. S. Yang, C. Q. Jin, and K. H. Kim, *New Journal of Physics* **2010**, 12.

(27) Y. S. Chai, Y. S. Oh, L. J. Wang, N. Manivannan, S. M. Feng, Y. S. Yang, L. Q. Yan, C. Q. Jin, and K. H. Kim, *Phys. Rev. B* **2012**, 85, 184406.

(28) T. Zhao, A. Scholl, F. Zavaliche, K. Lee, M. Barry, A. Doran, M. P. Cruz, Y. H. Chu, C. Ederer, N. A. Spaldin, R. R. Das, D. M. Kim, S. H. Baek, C. B. Eom, and R. Ramesh, *Nat Mater* **2006**, 5, 823-829.

(29) W. H. Meiklejohn and C. P. Bean, *Phys. Rev.* **1956**, 102, 1413-1414.

(30) W. H. Meiklejohn and C. P. Bean, *Phys. Rev.* **1957**, 105, 904-913.

Table of content